NANO LETTERS

2005
Vol. 5, No. 7
1503−1507

Electrochemical Tuning of Silver Nanoparticles Fabricated by Nanosphere Lithography

Xiaoyu Zhang, Erin M. Hicks, Jing Zhao, George C. Schatz, and Richard P. Van Duyne*

Department of Chemistry, Northwestern University, 2145 Sheridan Road, Evanston, Illinois 60208

Received May 10, 2005; Revised Manuscript Received June 11, 2005

ABSTRACT

An electrochemical method is developed to quantitatively modify and spectroscopically monitor the size and shape of Ag nanotriangles fabricated by nanosphere lithography (NSL) on an indium tin oxide (ITO) electrode surface. AFM and SEM results demonstrate that the preferential order of electrochemical oxidation for a nanotriangle is, surprisingly, bottom edges first, then triangular tips, then out-of-plane height.

Nanosphere lithography (NSL) is an inexpensive, simple to implement, high-throughput nanofabrication technique capable of producing a large variety of nanoparticle structures and well-ordered nanoparticle arrays.[1,2] This letter describes our recent efforts to broaden the scope of NSL by fabricating truncated tetrahedral Ag nanoparticles on indium tin oxide coated glass electrode surfaces. The samples produced have only small defect-free areas (1−2 μm^2) interspersed with a relatively large number of line defects (merged Ag nanotriangles). Nevertheless, it is shown that the simultaneous study of the optical and electrochemical properties of the Ag nanotriangles is possible. Well-ordered nanoparticle arrays on conducting transparent surfaces permit the simultaneous study of optical and electrochemical measurements. These new plasmonic materials enable the study of the effect of the electrochemical potential on the localized surface plasmon resonance (LSPR) of Ag nanopoarticles.[3] It should now be possible to develop electrochemical LSPR nanosensors.[4]

The LSPR is excited when a specific wavelength of light impinges on a noble metallic nanoparticle and causes the plasma of conduction electrons to oscillate collectively.[5] Because this collective oscillation of electrons occurs only for light within a certain bandwidth, noble metal nanoparticles exhibit selective photon absorption and resonant Rayleigh scattering, which can be monitored easily using UV−visible extinction spectroscopy. It is well established that the maximum extinction wavelength, λ_{max}, of the LSPR is strongly and systematically dependent upon the composition, size, shape, and interparticle spacing of nanoparticles.[6] Therefore, monitoring the LSPR λ_{max} permits in situ optical detection of changes in the Ag nanoparticle structure during electrochemical modification experiments.

Recently, it has been demonstrated that the LSPR λ_{max} of chemically reduced silver nanoparticles shifts ∼20−40 nm toward shorter wavelengths because of the increase in negative surface charge density on an ITO electrode surface with the application of potentials from 0 to −2 V (vs Ag/AgCl).[7,8] Poly(acrylic acid)[7,8] or aminobutylsiloxane[9] has been utilized to immobilize noble metal colloids onto ITO surfaces, which make it difficult to fabricate a well-ordered and repeatable surface motif, and therefore, to achieve controllable LSPR spectra.[10] Moreover, when anodic potentials were applied to silver colloid modified electrode surfaces, total dissolution of the colloids was observed.[11] In contrast, NSL-produced nanoparticle arrays have controlled shape, size, and interparticle spacing and are extremely stable to positive potentials applied on an ITO surface electrode that are less than the silver oxidation potential. This makes NSL-produced arrays a prime candidate for the use in the systematic study of electrochemical modification of nanoparticles.

This letter addresses two goals: (1) to develop a simple electrochemical method to modify the structure of NSL-fabricated silver nanoparticles and monitor these structure changes by in situ LSPR; and (2) to explore the electrochemical properties of Ag nanoparticles and other nanoscale materials.

ITO substrates (Delta Technologies Limited, Stillwater, MN) were cleaned by 10-min sonication in Detergent 8 (Alconox, Inc. New York, NY). $H_2O/NH_4OH/30\%$ H_2O_2 (5:1:1) with sonication for 1 h was used to render the ITO surface hydrophilic. Polystyrene nanospheres (Duke Scientific, Palo Alto, CA) were drop-coated onto the cleaned ITO substrates and were allowed to dry. This yielded a hexagonal

* Corresponding author. E-mail: vanduyne@chem.northwestern.edu. Tel: (847) 491−3516. Fax: (847) 491−7713.

10.1021/nl050873x CCC: $30.25
Published on Web 06/24/2005

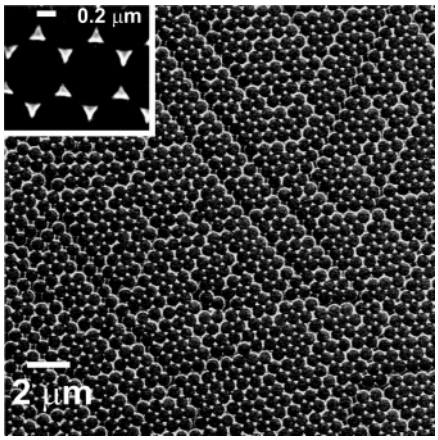

Figure 1. SEM images of Ag nanoparticle arrays on ITO. Nanosphere diameter $D = 590$ nm, the mass thickness of silver film $d_m = 67$ nm.

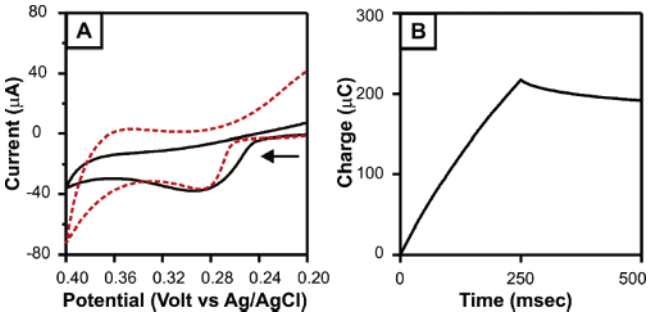

Figure 2. (A) Single-scan cyclic voltammograms of Ag film/ITO (dashed line, $d_m = 50 \pm 5$ nm) and Ag nanoparticle arrays on an ITO electrode (solid line) in 0.1 M $NaClO_4$ aqueous solution. Scan rate = 0.1 V/s. The arrow shows the initial scan direction. (B) Chronocoulometry plot of charge versus time for Ag nanoparticles on an ITO surface (0.64 cm^2) during the oxidation of Ag. Initial potential is 0.20 V, and the final potential is 0.40 V. Pulse width = 250 ms, $D = 590$ nm, $d_m = 67$ nm.

close-packed monolayer of nanospheres that served as the NSL deposition mask. The samples were mounted into a Consolidated Vacuum Corporation vapor deposition chamber. A Leybold Inficon XTM/2 quartz crystal microbalance was used to monitor the mass thickness, d_m, of the metal being deposited. Following metal deposition, the samples were sonicated for 1−2 min in ethanol (Pharmco, Evanston, IL) to remove the polystyrene nanosphere mask.

Scanning electron microscope (SEM) images were collected using a Hitachi S4500 field emission (Hitachi, Japan) electron microscope operating at an accelerating voltage of 5 kV and an average working distance of 7 mm. As shown in Figure 1, a well-ordered, minimal-defect Ag nanoparticle array on ITO with an area as large as ~400 μm^2 can be produced. The high-resolution, top-view SEM image (Figure 1 inset) clearly indicates that individual truncated Ag triangular nanoparticles have sharp tips. Additionally, the SEM studies demonstrate that the drop-coating fabrication method can easily achieve ~10% surface coverage of an Ag nanoparticle array monolayer with low defect density.

In this study, a BAS 100B/W electrochemical workstation was used for cyclic voltammetry and chronocoulometry measurements (Bioanalytical System Inc., West Lafayette, IN). The in-house constructed spectroelectrochemical cell consists of three electrodes with a Pt wire (D. F. Goldsmith, Evanston, IL) as the auxiliary electrode. All of the electrode potentials are reported versus an Ag/AgCl electrolyte reference electrode. Solutions were deoxygenated with nitrogen for a minimum of 2 min prior to electrochemical experiments. All of the electrochemical measurements were performed under an N_2 atmosphere.

Macroscale UV−visible extinction measurements were collected using a fiber-optically coupled Ocean Optics SD2000 (Ocean Optics, Dunedin, FL) spectrometer. All of the spectra in this study were macroscopic measurements performed in standard transmission geometry with unpolarized light. The light spot diameter was approximately 1 mm. The extinction maximum of each spectrum was located by calculating its first derivative.

Tapping-mode atomic force microscope (AFM) images were collected using a Digital Instruments Nanoscope IV microscope and Nanoscope IIIa controller (Digital Instruments, Santa Barbara, CA). Asymmetric phosphorus n-doped silicon tips (Veeco, Santa Barbara, CA, radius of curvature = 10 nm and resonant frequency = 304−385 kHz) were used to obtain all of the images.

The electrochemical oxidation of Ag nanoparticle arrays on an ITO electrode (Figure 2A, solid line) in an aqueous 0.1 M $NaClO_4$ solution was studied by single-sweep cyclic voltammetry (CV). The anodic scan (see arrow) was initiated at +200 mV, reversed to a cathodic scan at +400 mV, and terminated at +200 mV. The onset of the Ag nanoparticle oxidation, $Ag^0 \rightarrow Ag(I)^+ + e^-$, occurs at +240 mV, releasing $Ag(I)^+$ into solution and continues throughout the anodic scan. A parallel measurement (Figure 2A, dashed line) was carried out on a vapor-deposited Ag film/ITO electrode. The mass thickness, d_m, of the Ag film was 50 ± 5 nm. The onset of oxidation from the Ag film was +260 mV, in agreement with previous results.[12] In comparison, the cyclic voltammogram of the Ag nanoparticle arrays on an ITO electrode shows a broader peak, with a less positive onset potential. Clearly, some portion of the Ag nanoparticle arrays oxidize more easily than the bulk Ag film (Figure 2A, black solid line). Assuming that the surface free energy is the same for metal nanoparticles and bulk metal surfaces, the Kelvin equation[13] predicts that metal nanoparticles will exhibit a standard electrode potential, $E°$, that is shifted to more negative potentials than the $E°$ of the bulk metal.[14,15] A negative shift in $E°$ of small nanoparticles means that smaller metal nanoparticles are more easily oxidized than bulk material.[15−18]

A potential step from +200 mV to +400 mV was used in a chronocoulometry experiment to measure the charge required to oxidize the silver nanoparticles confined on the ITO surface (Figure 2B). Controllable tuning of the Ag nanoparticle structure was achieved by changing the electrochemical oxidation charge over the range of 10−1000 μC. In addition, the SEM studies (Figure 3) reveal the continued presence of well-ordered Ag nanoparticle arrays after repeated electrochemical oxidations, demonstrating high stability of Ag nanoparticle arrays on ITO.

A systematic study to relate electrochemically oxidized nanoparticle structures and optical properties was carried out

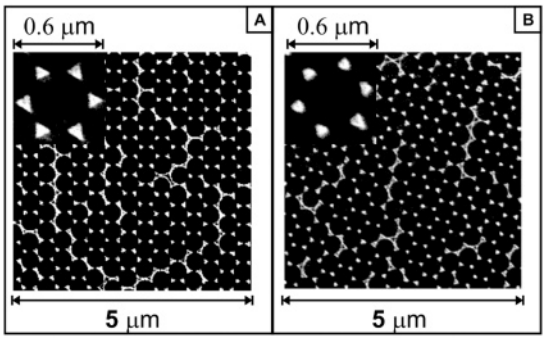

Figure 3. (A) SEM images of the nanoparticles before any electrochemical measurements. Sharp discrete triangles can be seen in the high-resolution inset. (B) SEM images of nanoparticles after one chronocoulometry measurement (electrochemical oxidation charge density ≈ 350 μC/cm^2). Rounding of the structure and a shrinking in the in-plane width of the nanoparticles can be seen. D = 390, d_m = 54 nm.

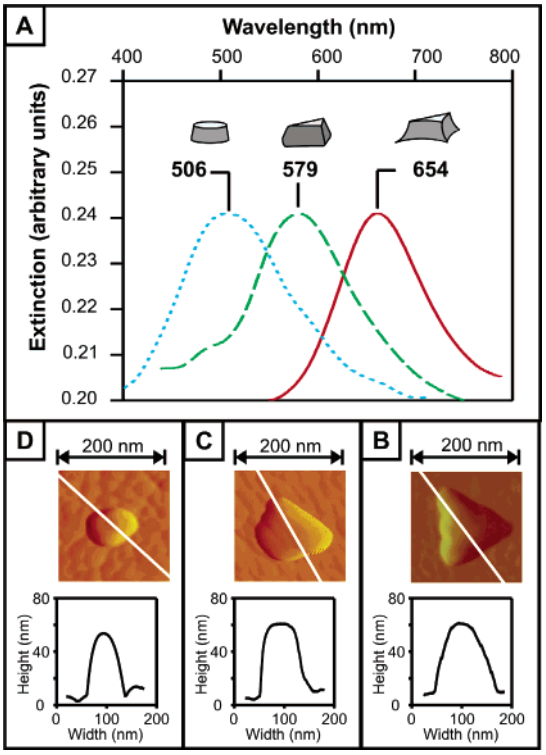

Figure 4. LSPR spectra and AFM images of Ag nanoparticles on ITO. D = 390 nm, d_m = 54 nm. (A) LSPR λ_{max} of the Ag nanoparticles shifts toward shorter wavelengths after chronocoulometry measurements. (B) AFM image before any electrochemical measurements. Average Ag nanoparticle out-of-plane height = 54 ± 2 nm, and in-plane width = 126 ± 12 nm. LSPR λ_{max} is 654 nm (solid line). (C) AFM image after one chronocoulometry measurement. Average Ag nanoparticle height = 52 ± 3 nm, and width = 87 ± 18 nm. LSPR λ_{max} is 579 nm (dashed line). (D) AFM image after two chronocoulometry measurements. Average Ag nanoparticle height = 45 ± 3 nm, and width = 76 ± 18 nm. LSPR λ_{max} is 506 nm (dotted line). All of the LSPR spectra were collected in an N_2 environment.

by combining LSPR spectroscopy and AFM. Figure 4 shows LSPR spectra and the corresponding AFM images of an Ag nanoparticle array on an ITO electrode during a succession of two measurements. Prior to electrochemical oxidation, the Ag nanoparticle arrays on an ITO electrode exhibit a LSPR λ_{max} at 654 nm (Figure 4A). With each successive chronocoulometry run, the plasmon peak shifts toward shorter wavelengths because of changes in the silver nanoparticle size and shape. Correlated AFM images were obtained to further characterize this geometry change of the nanoparticles. After the first chronocoulometry run (electrochemical oxidation charge density ~350 μC cm^{-2} ITO), the height of the nanoparticle remained unchanged; however, the base of the truncated tetrahedral structure became smaller and rounder, with a change of width from 126 ± 12 nm (Figure 4B) to 87 ± 18 nm (Figure 4C). This shape change is also evident in the SEM images (Figure 3). The 39-nm structural change in the in-plane width results in a shift in the LSPR spectra from 654 to 579 nm. Changes in the degree of tip sharpness have already been shown to change the position of the plasmon resonance dramatically.[19] This is because the highest electromagnetic field strength is located at the tips of the tetrahedral and triangular nanoparticles.[19,20]

After the second chronocoulmetry run (~40 μC/cm^2), the nanoparticles narrow in both the in-plane and out-of-plane direction and became hemispherical in shape (Figure 4D). The height was reduced from 52 ± 3 nm (Figure 4C) to 45 ± 3 nm (Figure 4D). The resulting plasmon at 506 nm is typical of a hemispherical nanoparticle as seen in earlier experiments.[21,22] After further electrochemical oxidation, the height of the nanoparticles was decreased further, and the plasmon blue-shifted out of the spectral range of the spectrometer (data not shown).

From Figure 4, we found that the electrochemical oxidation of an NSL-fabricated Ag nanoparticle began with the bottom edges. To further explore the oxidation preference between top tetrahedral tips and out-of-plane height, we selected a 590-nm nanosphere mask to create larger nanoparticles that allow relatively fine electrochemical control of nanoparticle sizes. Figure 5 illustrates the same series of observations presented in Figure 4 but for a larger nanoparticle size. The corresponding AFM measurements indicate that larger Ag nanoparticle arrays remain constant in height (~68 nm) throughout the two chronocoulometry runs. After the first chronocoulometry measurement (~300 μC/cm^2), the base of the truncated tetrahedral structure decreased from 231 to 201 nm, creating a trigonal prism structure (Figure 5C) in comparison to Figure 5B. Further electrochemical oxidation (~330 μC/cm^2) removed small amounts of silver from the truncated tetrahedral tips of the nanoparticle, while not changing the nanoparticle's out-of-plane height (Figure 5D). Comparing the studies done for both nanosphere sizes (Figures 4 and 5), the order of electrochemical oxidation of the truncated tetrahedral nanoparticles can be summarized as the following: bottom edges first, then top triangular tips, and finally out-of-plane height.

To understand this behavior, we note that Pleith[14] and Makov et al.[23] have studied the size-dependent electrochemical behavior of spherical nanoparticles previously, and they were able to rationalize their results assuming that the surface free energy makes a repulsive contribution to the electrochemical potential, which varies as the inverse of the nanosphere radius. In the present context, we would expect

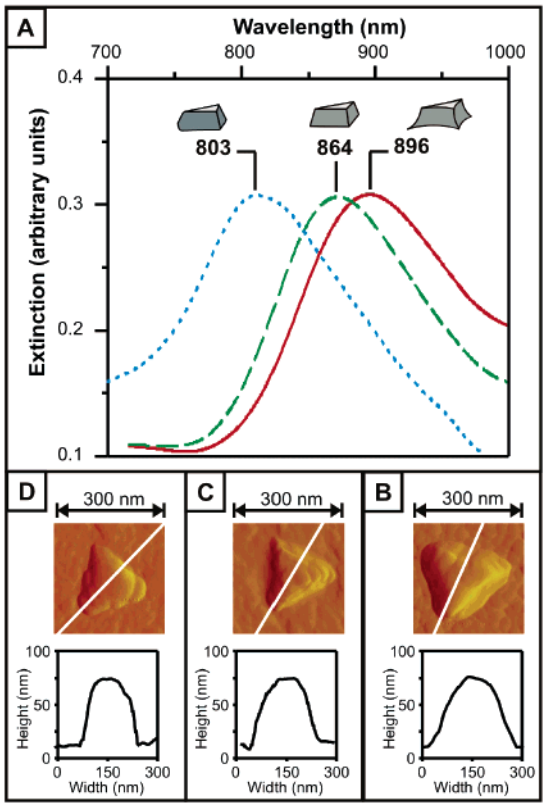

Figure 5. LSPR spectra and AFM images of Ag nanoparticles on ITO. D = 590 nm, d_m = 68 nm. (A) LSPR λ_{max} of the Ag nanoparticles shifts toward shorter wavelengths after chronocoulometry measurements. (B) AFM image before any electrochemical measurements. Average Ag nanoparticle out-of-plane height = 68 ± 2 nm, and in-plane width = 231 ± 16 nm. LSPR λ_{max} is 896 nm (solid line). (C) AFM image after one chronocoulometry measurement. Average Ag nanoparticle height = 68 ± 3 nm, and width = 201 ± 12 nm. LSPR λ_{max} is 864 nm (dashed line). (D) AFM after two chronocoulometry measurements. Average Ag nanoparticle height = 68 ± 3 nm, and width = 178 ± 10 nm. LSPR λ_{max} is 803 nm (dotted line). All of the LSPR spectra were collected in an N_2 environment.

that regions of the nanoparticle surface with the smallest radii of curvature should oxidize the most readily, so the bottom edges can precede the tips as long as the latter are sufficiently rounded (as seems to be the case from the AFM pictures).

Both the LSPR and AFM results indicate that the electrochemical oxidation method can easily modify the shape and size of silver nanoparticles confined on ITO. Moreover, the nanoparticle size/shape can be controlled quantitatively by tuning the electrochemical oxidation charge. To model this, we use Faraday's law

$$Q = nFN \tag{1}$$

along with the following formula that relates the oxidation-induced volume change to the number of coulombs of charge passed:

$$\Delta V_s = \frac{NMW_{Ag}}{\rho_{Ag} N_A A_{ITO}} = \frac{QMW_{Ag}}{nF\rho_{Ag} N_A A_{ITO}} \tag{2}$$

Here, Q is the charge; n is the number of electrons, which is 1 for the oxidation of $Ag^0(s)$ to $Ag(I)^+(aq)$; F is the Faraday constant; N is the quantity of oxidized silver in moles; ΔV_s is the change in volume of a single Ag nanoparticle; MW_{Ag} is the molecular formula weight of silver; ρ_{Ag} is the density of silver; N_A is the of number of Ag nanoparticles per 1 cm^2 ITO, which is ~7.2×10^8 Ag nanoparticles lying on a 1 cm^2 ITO surface on the basis of SEM measurements; and A_{ITO} is the ITO surface area in cm^2. On the basis of these expressions, after ~300 $\mu C/cm^2$ is passed through the Ag nanoparticle arrays on an ITO electrode (D = 590 nm, d_m = 68 nm, Figure 5B), ~4.6×10^4 nm^3 silver has been removed from an individual Ag nanoparticle.

We estimate the volume of the NSL-produced silver nanoparticle by assuming that the unoxidized nanoparticle has a truncated tetrahedral structure. The volume of the nanoparticle is

$$V_{bot} = V_{tetra} - V_{top} \tag{3}$$

where V_{tetra} is the volume of the tetrahedron constructed using the nanoparticle as the bottom of the tetrahedron and V_{top} is the volume of the top of the tetrahedron excluding the volume of the nanoparticle. V_{bot} can then be obtained by substituting the in-plane width of the nanoparticle, a_{bot}, and the out-of-plane height, h_{bot}, into the following equation (for the full derivation, refer to the Supporting Information):

$$V_{bot} = \frac{2\sqrt{6}}{27}[a_{bot}^3 - (a_{top})^3] \tag{4}$$

Here the in-plane width of the top tetrahedron is given by

$$a_{top} = a_{bot} - \frac{3\sqrt{2}}{4} h_{bot} \tag{5}$$

Using a_{bot} = 231 nm and h_{bot} = 68 nm, obtained from AFM measurements (Figure 5B), we determine the initial volume for an individual unmodified Ag nanoparticle to be ~1.5×10^6 nm^3. The volume after oxidation V'_{box} is then given by

$$V'_{bot} = V_{bot} - \Delta V_s \tag{6}$$

This volume can be used to estimate the oxidized nanoparticle structure (during the first phase of oxidation) by assuming that a_{top} and h_{bot} remain constant and the tetrahedron is oxidized only along its lower edge, converting the bottom of the nanoparticle into a trigonal prism whose in-plane width is a'_{bot}. This leads to the following expression for V'_{bot} (see the Supporting Information for details)

$$V'_{bot} = -\frac{4\sqrt{6}}{27} a'^{3}_{bot} + \frac{2\sqrt{6}}{9} a_{bot} a'^{2}_{bot} - \frac{2\sqrt{6}}{27} (a_{top})^3 \tag{7}$$

Solving this equation for a'_{bot}, an in-plane width of 206 nm

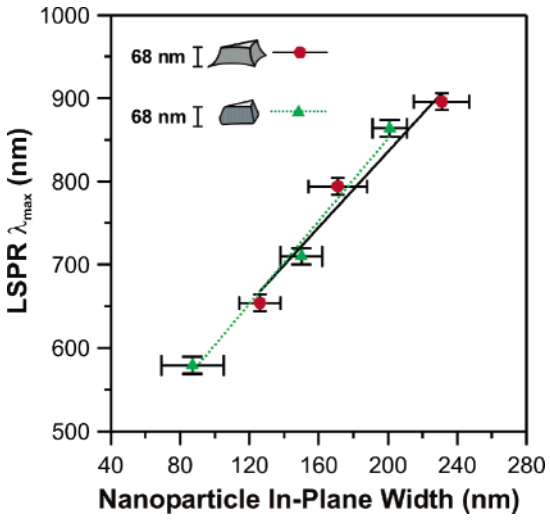

Figure 6. LSPR λ_{max} versus nanoparticle in-plane width. The nanoparticles were made from sphere masks using 390-, 510-. and 590-nm diameter spheres. The plots show data collected before (circles, solid line) and after electrochemical measurements (triangles, dotted line). The solid line ($R^2 = 0.97$) and dashed line ($R^2 = 0.99$) are the linear fits for each data set. The nanoparticles remained fixed at a height of 68 nm.

is calculated for the modified nanoparticle. This value is close to the AFM measurement, 201 ± 12 nm, given in Figure 5C.

To systematically study the relationship between nanoparticle width and plasmon λ_{max}, we carried out a set of experiments using masks created with the following nanosphere diameters: 390, 510, and 590 nm. This range of nanosphere sizes was chosen because the nanoparticles produced by NSL have plasmons in the range of 400−900 nm, the limiting range of the spectrometer. The initial height for the nanoparticles produced by each nanosphere mask was kept constant at 68 nm. After one chronocoulometry run, all of the modified nanoparticles still remained at a height of 68 nm. All of the height data were based on AFM measurements. The results of the study can be seen in Figure 6. There is a linear relationship between in-plane width and λ_{max} of the nanoparticles before and after electrochemical modifications. There is also a consistent blue-shift in the λ_{max} for each nanoparticle size after a single chronocoulometry run.

In summary, this work demonstrates the ability to produce large areas of monolayer Ag nanoparticle arrays on a transparent conductive substrate, the stability of NSL-produced Ag nanoparticle arrays on an ITO electrode in aqueous environments, the quantitative manipulation of Ag nanoparticle geometries by using chronocoulometry, and using LSPR spectroscopy for monitoring the manipulation.

Acknowledgment. We acknowledge Dr. Shengli Zou and Dr. Douglas A. Stuart at Northwestern University for helpful comments. This research was supported by the National Science Foundation (EEC-0118025, DMR-0076-97, CHE-0414554) and the Air Force Office of Scientific Research MURI program (F49620-02-1-0381).

Supporting Information Available: Detailed description of the derivation for obtaining the in-plane width of the modified nanoparticle is available. Also shown are two images defining the terms used in the derivation. This material is available free of charge via the Internet at http://pubs.acs.org.

References

(1) Hulteen, J. C.; Van Duyne, R. P. *J. Vac. Sci. Technol. A* **1995**, *13*, 1553.
(2) Haynes, C. L.; Van Duyne, R. P. *J. Phys. Chem. B* **2001**, *105*, 5599.
(3) Van Duyne, R. P. *Chemical and Biochemical Applications of Lasers*; Academic Press: New York, 1979; Vol. 4, p 101.
(4) Haes, A. J.; Van Duyne, R. P. *J. Am. Chem. Soc.* **2002**, *124*, 10596.
(5) Schatz, G. C.; Van Duyne, R. P. *Handbook of Vibrational Spectroscopy*; Wiley: New York, 2002; Vol. 1, p 759
(6) Kreibig, U.; Vollmer, M. *Metal Clusters*; Springer-Verlag: Heidelberg, Germany, 1995; Vol. 25.
(7) Chapman, R.; Mulvaney, P. *Chem. Phys. Lett.* **2001**, *349*, 358.
(8) Wang, Z.; Chumanov, G. *Adv. Mater.* **2003**, *15*, 1285.
(9) Toyota, A.; Nakashima, N.; Sagara, T. *J. Electroanal. Chem.* **2004**, *565*, 335.
(10) Gunnarsson, L.; Rindzevicius, T.; Prikulis, J.; Kasemo, B.; Käll, M.; Zou, S. L.; Schatz, G. C. *J. Phys. Chem. B* **2005**, *109*, 1079.
(11) Ung, T.; Giersig, M.; Dunstan, D.; Mulvaney, P. *Langmuir* **1997**, *13*, 1773.
(12) K'Owino, I. O.; Agarwal, R.; Sadik, O. A. *Langmuir* **2003**, *19*, 4344.
(13) Fisher, L. R.; Israelachvili, J. N. *J. Colloid Interface Sci.* **1981**, *80*, 528.
(14) Plieth, W. J. *J. Phys. Chem.* **1982**, *86*, 3166.
(15) Plieth, W. J. *Surf. Sci.* **1985**, *156*, 530.
(16) Ng, K. H.; Liu, H.; Penner, R. M. *Langmuir* **2000**, *16*, 4016.
(17) Chaki, N. K.; Sharma, J.; Mandle, A. B.; Mulla, I. S.; Pasricha, R.; Vijayamohanan, K. *Phys. Chem. Chem. Phys.* **2004**, *6*, 1304.
(18) Redmond, P. L.; Hallock, A. J.; Brus, L. E. *Nano Lett.* **2005**, *5*, 131.
(19) Jin, R.; Cao, Y.; Mirkin, C. A.; Kelly, K. L.; Schatz, G. C.; Zheng, J. G. *Science* **2001**, *294*, 1901.
(20) Haes, A. J.; Zou, S. L.; Schatz, G. C.; Van Duyne, R. P. *J. Phys. Chem. B* **2004**, *108*, 109.
(21) Jensen, T. R.; Duval Malinsky, M.; Haynes, C. L.; Van Duyne, R. P. *J. Phys. Chem. B* **2000**, *104*, 10549.
(22) Jensen, T. R.; Duval, M. L.; Kelly, L.; Lazarides, A.; Schatz, G. C.; Van Duyne, R. P. *J. Phys. Chem. B* **1999**, *103*, 9846.
(23) Makov, G.; Nitzan, A.; Brus, L. E. *J. Chem. Phys.* **1988**, *88*, 5076.

NL050873X